Tomographic reconstruction of "orphaned" oxygen orbitals in Li-rich battery material $Li_xTi_{0.4}Mn_{0.4}O_2$

Toward the achievement of a sustainable society, the electrification of mobility by means of lithium-ion technology is now gaining wider acceptance. However, the electrification of heavy-duty vehicles and aviation will require batteries with a much higher specific energy than that of existing lithium-ion batteries (LIBs). Each LIB is composed of an anode and a cathode immersed in an electrolyte and produces energy as lithium ions are shuttled between the two electrodes through a separator. The energy density of LIBs is determined by the combination of anode and cathode materials. Lithium metal and silicon are candidate materials for high-capacity anodes because they have theoretical capacities of 3860 $mAhg^{-1}$ and 4200 $mAhg^{-1}$, respectively. These values are about 10 times higher than that of a conventional graphite anode. On the other hand, for the cathode, there is an urgent need to find materials beyond those of the existing layered cathodes. Lithium-rich oxides present a promising class of cathode materials in this regard, with their high capacity of about 300 $mAhg^{-1}$ [1]. This capacity is significantly greater than that of conventional cathode materials; for example, $LiCoO_2$ has a capacity of 140 $mAhg^{-1}$, $LiMn_2O_4$ has a capacity of 120 $mAhg^{-1}$, and $LiFePO_4$ has a capacity of 170 $mAhg^{-1}$. Such capacities of lithium-rich oxides have been suggested to result from a combination of cationic and anionic redox processes. The conventional cathode materials such as $LiCoO_2$ and $LiFePO_4$ involve only the cationic redox reaction; therefore, it has been difficult to increase the capacity. The anionic redox mechanism underlying the electrochemical process of lithium-rich oxides, however, has been difficult to understand fully using only the known probes and techniques. In this research, using high-energy X-ray Compton measurements together with first-principles modeling, we show how the electronic orbital that lies at the heart of the reversible and stable anionic redox activity can be imaged and visualized, and its character and symmetry are determined. Our results not only provide a picture of the workings of a lithium-rich battery at the atomic scale but also suggest pathways to improving existing battery materials and designing new ones [2].

High-energy X-ray Compton scattering experiments were performed at SPring-8 **BL08W**. The sample is the cation-disordered rock salt $Li_xTi_{0.4}Mn_{0.4}O_2$ (lithium concentration x = 0, 0.4, 0.8, and 1.2). This material is attracting attention as a lithium-rich oxide that has a high capacity of more than 300 $mAhg^{-1}$ even though it does not include rare metals. The lithium concentration of $Li_xTi_{0.4}Mn_{0.4}O_2$ was changed chemically. In this material, it has been reported that the cationic redox reaction is dominant over the lithium concentration range of $0 < x < 0.4$, whereas the anionic redox reaction is dominant over the lithium concentration range of $0.4 < x < 1.2$ [3]. The change from the cationic to the anionic redox reaction at around x = 0.4 has also been confirmed by the spin magnetic moment obtained from magnetic Compton scattering studies [4].

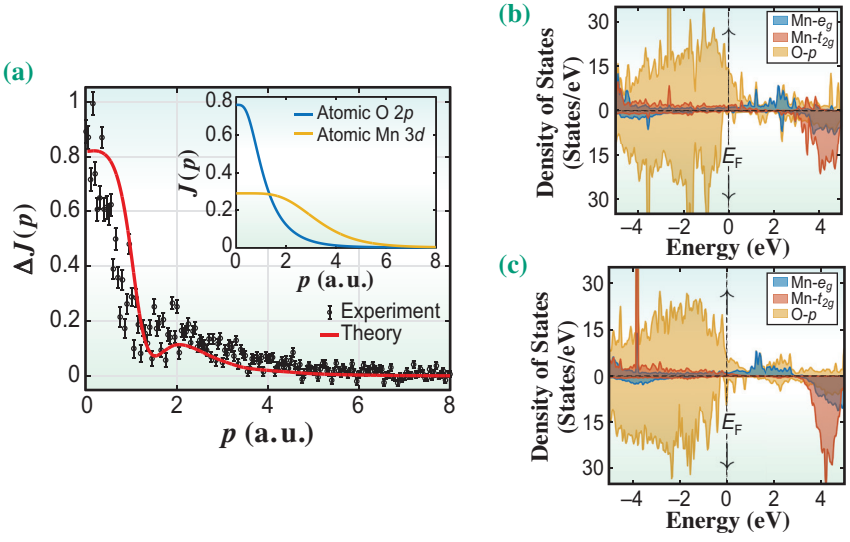

Fig. 1. **(a)** Difference Compton profiles between materials with lithium concentrations of x = 0.4 and 0.8. The solid line is a theoretical difference Compton profile obtained by the first-principles calculation. The inset shows theoretical Compton profiles of O 2p and Mn 3d orbitals obtained by atomic model calculation. **(b)** and **(c)** show spin-dependent partial densities of states for x = 0.4 and 0.8, respectively. The dashed line shows Fermi energy.

Figure 1(a) shows the difference Compton profile corresponding to the difference in the profiles of $Li_xTi_{0.4}Mn_{0.4}O_2$ with x = 0.8 and 0.4. The solid line in Fig. 1 is the theoretical difference Compton profile obtained by the first-principles density functional theory (DFT)-based modeling of lithium-rich battery materials. The comparison of the experimental and theoretical difference Compton profiles reveals the presence of O 2*p* anionic states in the range of electron momentum $p_z < 2$ atomic units. The long tail in the difference Compton profiles can be explained by the transfer of about 0.19 of Mn 3*d* electrons from the delocalized to localized 3*d* states. This localization is caused by the Coulomb repulsion between an occupied state at the O site and the 3*d* states in the neighboring Mn ions, without the formation of a substantial covalent bond. Therefore, the O 2*p* orbital appears to be orphaned [5]. Figures 1(b) and 1(c) show the spin-dependent partial densities of states (PDOSs) associated with Mn e_g, Mn t_{2g}, and O *p* orbitals for x = 0.4 and 0.8, respectively. The PDOS for x = 0.4 shows the presence of a peak of a localized hole state right above the Fermi level, as shown in Fig. 1(b).

Figure 2(a) shows two-dimensional electron momentum densities (2D-EMDs) for the redox orbitals, which are one-dimensional integrals along a crystallographic axis of the three-dimensional EMD. The features in Fig. 2(a) reveal the presence of repulsive Coulomb (nonbonding) interactions between the O 2*p* and Mn t_{2g} orbitals. A weak π-type antibonding interaction exists between the O 2*p* and Mn t_{2g} orbitals, as shown in the left-side diagram in Fig. 2. Sharp box-like features (colored light blue) in the high-momentum region are associated with Fermi surface breaks related to the t_{2g} band. In contrast, the repulsive Coulomb interaction produces a substantial delocalization of O 2*p* orbitals in momentum space (or localization in real space) in comparison with the redox orbital in the spinel material $Li_xMn_2O_4$ (Fig. 2(b)). In the spinel case, the O 2*p* orbitals are modified by the covalent bond involving the e_g states on the Mn atoms, which induces them to localize in momentum space (or to delocalize in real space). The visualization of the interaction between the O 2*p* and transition metal t_{2g} electrons to estimate the number of electrons displaced by the Coulomb interaction provides useful descriptors for designing stable, high-capacity oxygen-redox electrode materials. Our study enables the direct visualization of the orbitals involved in the anionic redox processes and offers quantitative analyses based on new descriptors derived from the electron momentum density.

In this study, we revealed the anionic redox mechanism and visualized the nonbonding O 2*p* redox orbital in a lithium-rich battery material, $Li_xTi_{0.4}Mn_{0.4}O_2$, by combining high-energy X-ray Compton measurements and first-principles calculations. The obtained results are based on the bulk sensitivity of Compton scattering technique using high-energy synchrotron X-rays. A detailed understanding of the redox mechanism on an atomic scale will pave the way to improving existing battery materials and designing new ones.

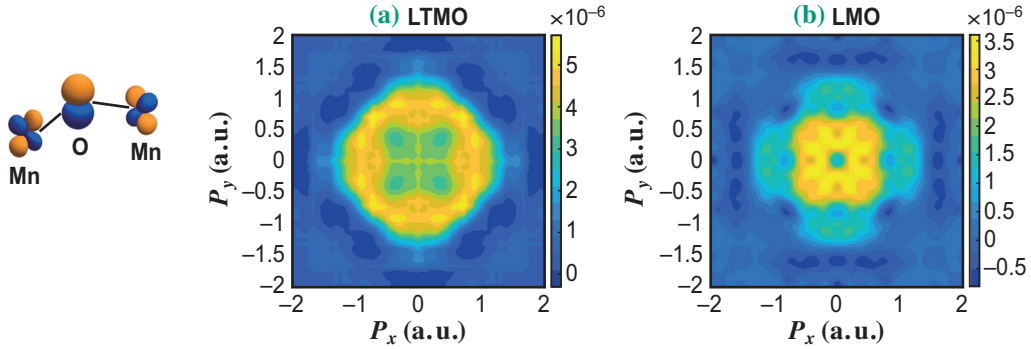

Fig. 2. **(a)** Reconstructed electron momentum density map of the O 2*p* orbital in $Li_xTi_{0.4}Mn_{0.4}O_2$ with x = 0.8 and 0.4. **(b)** Reconstructed electron momentum density map of the O 2*p* orbital in $Li_xMn_2O_4$ with x = 1.079 and 0.496. The left-side diagram shows O 2*p* and Mn t_{2g} orbitals. A weak π-type antibonding interaction exists between the O 2*p* and Mn t_{2g} orbitals, and this interaction causes the nonbonding O 2*p* state in (a).

Kosuke Suzuki[a,*] and Hasnain Hafiz[b]

[a] Graduate School of Science and Technology, Gunma University
[b] Department of Mechanical Engineering, Carnegie Mellon University, USA

*Email: kosuzuki@gunma-u.ac.jp

References

[1] G. Assat *et al.*: Nat. Energy **3** (2018) 373.
[2] *H. Hafiz, K. Suzuki, B. Barbiellini, N. Tsuji, N. Yabuuchi, K. Yamamoto, Y. Orikasa, Y. Uchimoto, Y. Sakurai, H. Sakurai, A. Bansil, V. Viswanathan.: Nature* ***594*** *(2021) 213.*
[3] N. Yabuuchi *et al.*: Nat. Commun. **7** (2016) 13814.
[4] K. Suzuki *et al.*: Condens. Matter **7** (2022) 4.
[5] M. Okubo *et al.*: ACS Appl. Mater. Interfaces **9** (2017) 36463.